

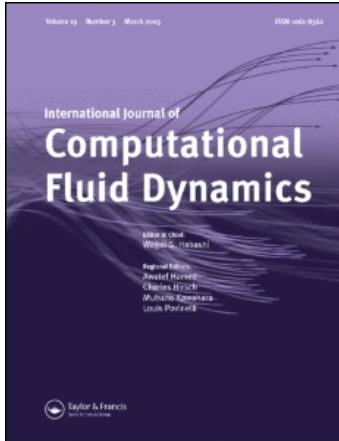
This article was downloaded by: [Sugiyama, Hitoshi]

On: 25 November 2010

Access details: Access Details: [subscription number 930116579]

Publisher Taylor & Francis

Informa Ltd Registered in England and Wales Registered Number: 1072954 Registered office: Mortimer House, 37-41 Mortimer Street, London W1T 3JH, UK



## International Journal of Computational Fluid Dynamics

Publication details, including instructions for authors and subscription information:

<http://www.informaworld.com/smpp/title~content=t713455064>

### Numerical analysis of turbulent flow in a rotating U-bend with roughened walls

Hitoshi Sugiyama<sup>a</sup>; Chiriki Watanabe<sup>b</sup>; Naoto Kato<sup>a</sup>

<sup>a</sup> Department of Mechanical Engineering, Utsunomiya University, Utsunomiya, Japan <sup>b</sup> Honda Engineering Co. Ltd, Utsunomiya, Japan

Online publication date: 24 November 2010

**To cite this Article** Sugiyama, Hitoshi , Watanabe, Chiriki and Kato, Naoto(2010) 'Numerical analysis of turbulent flow in a rotating U-bend with roughened walls', International Journal of Computational Fluid Dynamics, 24: 8, 335 – 348

**To link to this Article:** DOI: 10.1080/10618562.2010.531685

**URL:** <http://dx.doi.org/10.1080/10618562.2010.531685>

PLEASE SCROLL DOWN FOR ARTICLE

Full terms and conditions of use: <http://www.informaworld.com/terms-and-conditions-of-access.pdf>

This article may be used for research, teaching and private study purposes. Any substantial or systematic reproduction, re-distribution, re-selling, loan or sub-licensing, systematic supply or distribution in any form to anyone is expressly forbidden.

The publisher does not give any warranty express or implied or make any representation that the contents will be complete or accurate or up to date. The accuracy of any instructions, formulae and drug doses should be independently verified with primary sources. The publisher shall not be liable for any loss, actions, claims, proceedings, demand or costs or damages whatsoever or howsoever caused arising directly or indirectly in connection with or arising out of the use of this material.

## Numerical analysis of turbulent flow in a rotating U-bend with roughened walls

Hitoshi Sugiyama<sup>a\*</sup>, Chiriki Watanabe<sup>b</sup> and Naoto Kato<sup>a</sup>

<sup>a</sup>Department of Mechanical Engineering, Utsunomiya University, Utsunomiya, Japan; <sup>b</sup>Honda Engineering Co. Ltd, Utsunomiya, Japan

(Received 4 September 2009; final version received 11 October 2010)

A numerical analysis has been performed for a developing turbulent flow in a rotating U-bend of strong curvature with rib-roughened walls using an anisotropic turbulent model. In this calculation, an algebraic Reynolds stress model is used to precisely predict Reynolds stresses, and a boundary-fitted coordinate system is introduced as a method of coordinate transformation to set the exact boundary conditions along the complicated shape of U-bend with rib-roughened walls. Calculated results for mean velocity and Reynolds stresses are compared to the experimental data in order to validate the proposed numerical method and the algebraic Reynolds stress model. Although agreement is certainly not perfect in all details, the present method can predict characteristic velocity profiles and reproduce the separated flow generated near the outer wall, which is located just downstream of the curved duct. The Reynolds stresses predicted by the proposed turbulent model agree well with the experimental data, except in regions of flow separation.

**Keywords:** numerical analysis; turbulent flow; algebraic Reynolds stress model; rotation; roughened wall; U-bend; boundary-fitted coordinate system

### 1. Introduction

Heat transfer augmentation inside internal channels of an airfoil is an important consideration in the gas turbine industry. Advanced gas turbine blades have been designed to operate at high inlet temperatures, which far exceed the allowable metal temperatures. Therefore, the turbine blades must be cooled efficiently in order to maintain the performance of the turbine. In the case of internal cooling of the blades, cool air extracted from the compressor stages of the engine is circulated through internal cooling passages inside the turbine rotor blades, in order to maintain the operating temperature of the blades at safe levels. At the same time, heat transfer augmentation is achieved using roughened walls as turbulence promoters. The roughened walls have rib positioned at intervals that produce a complex flow field involving flow separation and reattachment between the ribs, which produces a high turbulence level that leads to high-heat transfer coefficients. The flow development and the heat transfer characteristics inside these cooling passages are affected by the presence of sharp U-bends, the rotation of the blades and the presence of heat transfer enhancing ribs. Detailed information about the flow and heat transfer characteristics in a ribbed channel is important in the design of gas turbine engines.

In the experimental investigation reported in the literature, the internal cooling passages of the gas

turbine have been modelled as either square or rectangular ducts having two opposite walls equipped with cyclic ribs. The effects of geometric parameters such as relative rib height, relative rib pitch, angle of attack, duct aspect ratio, rib cross-section geometry and rib configuration have been investigated extensively. One of the earliest experimental studies was conducted by Burggraf (1970), who investigated the turbulent flow in a square duct with two opposite ribbed walls. Han *et al.* (1988) reported the mass transfer distributions around sharp 180° turns in a two-pass, square, smooth channel and in an identical channel with two rib-roughened opposite walls obtained using the naphthalene sublimation technique. Ekkad *et al.* (2000) reported detailed heat transfer distributions inside a two-pass coolant channel with cross-flow induced by swirling and impingement using liquid crystals. Hsieh *et al.* (1999) measured an approximately two-dimensional turbulent flow in a rotating two-pass channel of square cross-section without ribs by applying laser-Doppler anemometry. They reported the measured flow field to be quite complex, consisting of secondary flow and radical outward flow due to Coriolis effects and centrifugal forces. Iacovides *et al.* (1996) reported detailed measurements of turbulent flows in a square sectioned 180° sharp turn of a coolant passage with and without rotation obtained by laser-Doppler anemometry, including Reynolds stress distributions. They

\*Corresponding author. Email: sugiyama@cc.utsunomiya-u.ac.jp

concluded that orthogonal rotation transfers high-momentum fluid towards the duct pressure side, augments the pressure-side turbulence levels and suppresses suction-side turbulence. Iacovides *et al.* (1999) also examined the effects of the location of the first outer-wall rib after the bend exit. They presented detailed near-wall, mean and turbulent flow data, which provide information on the secondary motion and the three-dimensionality of the flow.

Numerical analyses of turbulent flow in a sharp-turn channel with roughened walls have also been performed using various turbulent models. Iacovides and Raisee (1999) presented computational results for turbulent flow and heat transfer in a rib-roughened U-bend without rotation. They compared calculated mean velocity and temperature distributions to experimental data and concluded that the second moment closure model must be used in order to correctly reproduce the flow separation and that low-Reynolds-number turbulence models are needed for thermal predictions. Jang *et al.* (2001) presented calculated results for the turbulent flow and heat transfer for a two-pass square channel with and without 60° angled parallel ribs. They used the finite analytic method, which solves the Reynolds-averaged Navier–Stokes equation in conjunction with a near-wall second-order Reynolds stress closure model, and a two-layer  $k$ - $\varepsilon$  isotropic eddy viscosity model. Comparing the second-moment and two-layer calculations with the experimental data demonstrated that angled rib turbulators and the 180° sharp turn of the channel produced strong non-isotropic turbulence, which significantly affected the flow field and heat transfer coefficients. Sugiyama and Watanabe (2003) reported calculated results for turbulent flows in a square-sectioned 180° sharp turn without rotation, which were measured by Iacovides *et al.* (1996). Calculated results for mean velocity and Reynolds stresses are compared to the experimental data in order to examine the validity of the algebraic Reynolds stress model. They concluded that the proposed turbulent model could predict velocity profiles correctly and could reproduce the separated flow generated near the outlet cross-section of the curved duct. Recently, Guleren and Turan (2007) presented the numerical results of the developing turbulent flow through stationary and rotating U-bends with strong curvature using large-eddy simulation. However, the U-duct was composed of smooth walls without ribs. They reported that the agreement between the predictions and the experimental data is quite satisfactory, considering the coarse grid that was adopted.

Very few computational studies have been performed on rotating sharp-turn channels with roughened walls. Iacovides (1999) calculated the turbulent

flows through stationary and rotating U-bends of square cross-section, with rib-roughened inner and outer walls along the straight sections. Comparison of the calculated results with the experimental data suggested that a low-Reynolds-number second-moment closure is necessary in order to reliably predict the region of flow separation induced by strong curvature and the presence of ribs. Lin *et al.* (2001) predicted the turbulent flow and heat transfer in a U-bend of square cross-section under rotating and non-rotating conditions using a low-Reynolds-number two-equation turbulent model. They reported that the secondary flows generated by Coriolis force and centrifugal buoyancy in the upper straight duct can have a strong effect on the secondary flows induced by the ribs.

As mentioned above, the turbulent flow and heat transfer in internal cooling passages inside turbine rotor blades have been investigated in numerous experimental and numerical studies. Few numerical results have been reported for turbulent flows in rotating sharp-turn channels with roughened walls, as compared to turbulent flows in stationary sharp-turn channels. Moreover, there have been few detailed reports on the distributions of Reynolds stresses in rotating sharp-turn channels with roughened walls. Therefore, the goal of the present study is to predict the turbulent flow in a rotating sharp-turn channel with roughened walls using an algebraic Reynolds stress model, which is able to correctly reproduce anisotropic turbulent flow. In order to confirm the validity of the proposed method and turbulence model, the calculated results are compared to the experimental data reported by Iacovides *et al.* (1996).

## 2. Numerical method

### 2.1. Numerical subject and definition of coordinate system

A schematic diagram of the rotating U-bend with roughened walls developed by Iacovides *et al.* (1996) is shown in Figure 1. A rotating U-bend of 0.05-m square cross-section and with a bend curvature ratio,  $Rc/D$ , of 0.65 is mounted on a turntable such that the curvature axis of the duct is parallel to the axis of rotation. The inner and outer duct walls of the upstream and downstream sections are artificially roughened by the placement of ribs of square cross-section in a staggered arrangement. The distance between the inlet cross-section of the upstream straight duct and the first rib is 3.5  $D$ . These ribs are oriented normal to the duct axis. The rib-height to duct diameter ratio,  $h/D$ , is 0.1, and the pitch to height ratio,  $P/h$ , is 10. The rest of walls except for roughened walls of the square duct were smooth

walls. Iacovides *et al.* (1996) measured the turbulent flow in a rotating U-bend in detail using a laser Doppler anemometer and presented the distributions of mean velocity and Reynolds stresses. Water was used as the working fluid. They measured the turbulent flows for three cases for a flow Reynolds number of 100,000: stationary U-bend, a U-bend rotating in the clockwise (positive) direction at  $Ro = 0.2$ , and U-bend in the counterclockwise (negative) direction at  $Ro = -0.2$  as viewed from above, as shown in Figure 1. In all cases, traverses were carried out both within the U-bend and within the upstream and downstream straight ducts. These traverses enabled measurement of mean velocity components in the streamwise and cross-duct directions, measurement of the corresponding turbulent intensities and shear stresses, and measurement of the four triple correlations associated with these directions.

The coordinate system used in the calculation is also defined in Figure 1. For convenience, rectangular and cylindrical coordinates are adopted in the straight and curved ducts, respectively. In the straight duct, the streamwise flow direction is along the  $X_1$  axis, and the secondary flow directions are along the  $X_2$  and  $X_3$  axes,

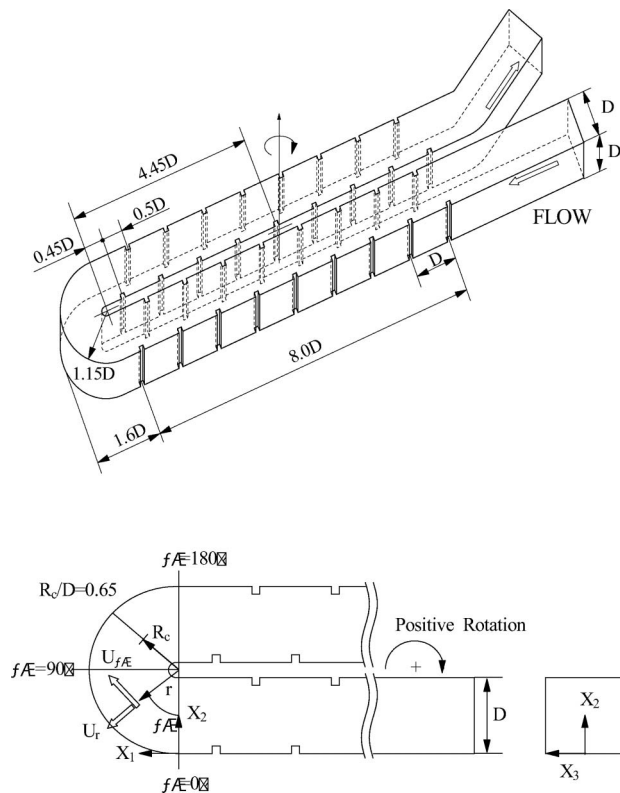


Figure 1. Schematic diagram of a rotating U-bend with roughened walls and definition of coordinate system.

which represent the vertical and horizontal directions to the roughened walls, respectively. The origin of the rectangular coordinates is set at the middle of the outer wall of the inlet cross-section of the curved duct. In addition, the upstream and downstream straight ducts are distinguished by the sign of the  $X_1$  axis, i.e.  $-X_1$  and  $X_1$  denote the upstream and downstream straight ducts, respectively.

The locations of the measurement cross-sections are shown in Figure 2. The calculated results are compared to the experimental data for mean velocity and Reynolds stresses. The locations of the measurement cross-sections are given in terms of  $X_1/D$  and bend angle  $\theta$ .

### 2.2. Governing transport equation

The transport equation of momentum is expressed through ensemble averaging in the case of rotating coordinates, as follows:

$$\frac{D(U_i U_j)}{Dt} = -\frac{1}{\rho} \frac{\partial P}{\partial X_i} + \frac{\partial}{\partial X_j} \left[ \nu \left( \frac{\partial U_i}{\partial X_j} + \frac{\partial U_j}{\partial X_i} \right) - \overline{u_i u_j} \right] - 2\varepsilon_{ijp} \Omega_p U_j - (\Omega_j X_j \Omega_i - \Omega_j X_i \Omega_j). \quad (1)$$

The third and fourth terms of the right-hand side of Equation (1) represent the Coriolis and centrifugal forces induced by rotation, respectively. In this equation,  $\Omega_i$  is the angular velocity of the duct about the  $X_i$  axis. The Reynolds stresses  $\overline{u_i u_j}$  that appear in the transport equation must be solved in order to obtain the velocity fields completely. In this calculation, we have adopted the transport equation of Reynolds stresses in order to accurately predict anisotropic turbulence. The transport equation of Reynolds stresses is given in the following form:

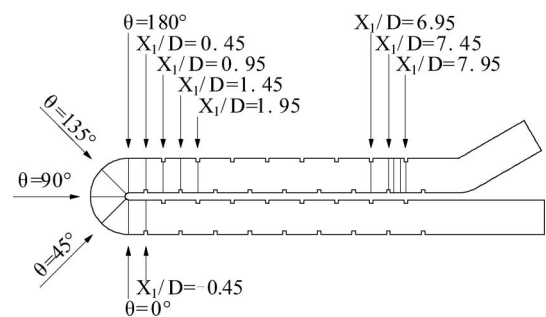


Figure 2. Measurement positions in the U-bend with roughened walls.

$$\begin{aligned} \frac{D\overline{u_i u_j}}{Dt} = & - \left( \overline{u_i u_k} \frac{\partial U_j}{\partial X_k} + \overline{u_j u_k} \frac{\partial U_i}{\partial X_k} \right) + \frac{p}{\rho} \left( \frac{\partial u_i}{\partial X_j} + \frac{\partial u_j}{\partial X_i} \right) \\ & - \frac{\partial}{\partial X_k} \left\{ \overline{u_i u_j u_k} - v \frac{\partial \overline{u_i u_j}}{\partial X_k} + \frac{p}{\rho} (\delta_{jk} u_i + \delta_{ik} u_j) \right\} \\ & - 2\Omega_k (\overline{u_j u_m} \varepsilon_{ikm} + \overline{u_i u_m} \varepsilon_{jkm}) \\ & - 2v \frac{\partial u_i}{\partial X_k} \frac{\partial u_j}{\partial X_k}. \end{aligned} \quad (2)$$

The fourth term of the right-hand side is the production term generated by rotation. Since the above equation cannot be directly solved numerically, several of the terms of the Reynolds stress equation must be rewritten by introducing the concept of the turbulent model. Moreover, with respect to the numerical analysis, the convection term of the left-hand side and the diffusion term of right-hand side of Equation (2) make it difficult to obtain a numerical solution because these terms require iterative calculation in order to obtain stable results. In the present study, these terms are modelled by adopting Rodi's (1976) approximation. As a result of this approximation, these two terms are transformed from difference form into algebraic form. Therefore, the convection and diffusion terms in the above equation were modelled as follows:

$$\frac{D\overline{u_i u_j}}{Dt} - Diff_{ij} = \frac{\overline{u_i u_j}}{2k} (P_k - \varepsilon) \quad (3)$$

where  $Diff_{ij}$  corresponds to the third term of the right-hand side of Equation (2), and  $P_k$  and  $\varepsilon$  represent the production term of the turbulent energy equation and dissipation, respectively.

A particularly problematic task is the modelling of the pressure-strain correlation equation term, which is also defined as the redistribution term and is shown as the second term of the right-hand side of Equation (1). The pressure-strain term is composed of three parts, which are the interaction of fluctuating velocities ( $\pi_{ij,1} + \pi_{ji,1}$ ), the interaction of the mean strain with fluctuating velocities ( $\pi_{ij,2} + \pi_{ji,2}$ ) and wall proximity effects ( $\pi_{ij,w} + \pi_{ji,w}$ ). In the present calculation, we have adopted Rotta's linear return to isotropy mode for the term ( $\pi_{ij,1} + \pi_{ji,1}$ ), as shown in Table 1.

For  $\pi_{ij,2}$ , the correlation is approximated as

$$\pi_{ij,2} = \left( \frac{\partial U_l}{\partial X_m} \right) a_{lj}^{mi} \quad (4)$$

and  $a_{lj}^{mi}$  is the fourth-order tensor, which should satisfy the following kinematic constraints:

$$a_{lj}^{mi} = a_{lj}^{im} = a_{ji}^{im} \quad (5)$$

$$a_{lj}^{mi} \frac{\partial U_l}{\partial X_m} = 0 \quad (6)$$

$$a_{jj}^{mi} = 2\overline{u_m u_i}. \quad (7)$$

The above constraints arise from the symmetry condition, the mass conservation law and Green's theorem, respectively. Although the kinematic constraint of Equation (6) differs from the constraint presented by Launder *et al.* (1975), we adopted Equation (6) because  $\pi_{ij,2}$  is defined as the production between the fourth-order tensor and the mean strain, as shown in Equation (4). Gessner and Eppich (1981) also reported these constraints and described them in detail. In terms of the modelling of ( $\pi_{ij,2} + \pi_{ji,2}$ ), the modelling process is described in detail in a previous report by Sugiyama and Hitomi (2005). Finally, the interaction of the mean strain and fluctuating velocities ( $\pi_{ij,2} + \pi_{ji,2}$ ) is modelled as shown in Table 1.

The wall effect term ( $\pi_{ij,w} + \pi_{ji,w}$ ) of the turbulent stresses is modelled, as shown in Table 1, by varying the model constants. In Table 1,  $f(L/X_w)$  is a function that is related to the dimensionless distance from the wall, and  $C_\mu$  and  $\kappa$  represent the empirical constant and the von Karman constant, respectively. The function  $f(L/X_w)$  takes unit value near the wall and approaches zero with increasing distance from the wall. The symbol  $X_w$  is the normal distance from the wall, and  $L$  defines the length scale of turbulence. When  $f(L/X_w)$  takes zero value, the model yields the correct Reynolds stress components for the nearly homogeneous shear flow of Champagne *et al.* (1970), whereas  $f(L/X_w)$  has unit value, and the magnitude of the stress components agree with the consensus of near

Table 1. Modeling of the pressure-strain correlation term.

$\pi_{ij,1} + \pi_{ji,1}$	$-C_1 \frac{\varepsilon}{k} \left( \overline{u_i u_j} - \frac{2}{3} k \delta_{ij} \right)$
$\pi_{ij,2} + \pi_{ji,2}$	$-\frac{C_2 + 8}{11} \left( P_{ij} - \frac{2}{3} P_k \delta_{ij} \right) + \zeta k \left( \frac{\partial U_i}{\partial X_j} + \frac{\partial U_j}{\partial X_i} \right) - \frac{8C_2 - 2}{11} \left( D_{ij} - \frac{2}{3} P_k \delta_{ij} \right)$
$[\pi^{ij} + \pi^{ji}]$	$C_1 = C_1^* + C_1' f\left(\frac{L}{X_w}\right) \quad C_2 = C_2^* + C_2' f\left(\frac{L}{X_w}\right) \\ \zeta = \zeta^* + \zeta' f\left(\frac{L}{X_w}\right)$
$P_{ij} = -\overline{u_i u_k} \frac{\partial U_j}{\partial X_k} - \overline{u_j u_k} \frac{\partial U_i}{\partial X_k}$	$D_{ij} = -\overline{u_i u_k} \frac{\partial U_k}{\partial X_j} - \overline{u_j u_k} \frac{\partial U_k}{\partial X_i}$
$P_k = -\overline{u_k u_l} \frac{\partial U_k}{\partial X_l}$	$f\left(\frac{L}{X_w}\right) = \frac{C_\mu^{\frac{3}{4}} k^{\frac{3}{2}}}{\kappa \varepsilon X_w}$

wall turbulence. The model constants used in this analysis are summarised in Table 2. After setting these model constants based on the basic experimental data, these coefficients have never been tuned in any cases of calculations.

The fourth term of the right-hand side of Equation (2) is the homogeneous part of the dissipation. The dissipation rate everywhere in the computed flow was assumed to be locally isotropic, i.e.

$$\varepsilon_{ij} = 2\nu \frac{\partial u_i}{\partial X_k} \frac{\partial u_j}{\partial X_k} = \frac{2}{3} \delta_{ij} \varepsilon. \tag{8}$$

The transport equations of turbulent energy and dissipation are expressed as follows:

$$\frac{Dk}{Dt} = \frac{\partial}{\partial X_j} \left\{ \left( \nu \delta_{jk} + c_s \frac{k}{\varepsilon} \overline{u_k u_j} \right) \frac{\partial k}{\partial X_k} \right\} - \overline{u_i u_k} \frac{\partial U_i}{\partial X_k} - \varepsilon \tag{9}$$

$$\begin{aligned} \frac{D\varepsilon}{Dt} = & \frac{\partial}{\partial X_j} \left\{ \left( \nu \delta_{jk} + c_\varepsilon \frac{k}{\varepsilon} \overline{u_k u_j} \right) \frac{\partial \varepsilon}{\partial X_k} \right\} \\ & - \frac{\varepsilon}{k} \left( c_{1\varepsilon} \overline{u_i u_k} \frac{\partial U_i}{\partial X_k} + c_{2\varepsilon} \varepsilon \right) \end{aligned} \tag{10}$$

where model constants  $c_s$ ,  $c_\varepsilon$ ,  $c_{1\varepsilon}$  and  $c_{2\varepsilon}$  are 0.22, 0.18, 1.44 and 1.92, respectively.

**2.3. Boundary-fitted coordinate system**

Calculation requires the boundary condition to be set precisely along a complicated shape. The boundary-fitted coordinate system is a kind of coordinate transformation method. The coordinate in the physical plane can be transformed into the coordinate in the calculation plane using the boundary-fitted coordinate system. Numerical calculation is performed in the calculation plane because it is easy to set the boundary condition along a complicated shape in the calculation plane. In addition, the governing equations are transformed from the simple equations expressed in the physical plane into complicated equations, even though it is easy to set the boundary condition along a complicated shape.

The transformation from the physical plane to the calculation plane is performed using the following mathematics theorem:

$$\frac{\partial}{\partial X_i} = \frac{\partial \xi}{\partial X_i} \frac{\partial}{\partial \xi} + \frac{\partial \eta}{\partial X_i} \frac{\partial}{\partial \eta} + \frac{\partial \zeta}{\partial X_i} \frac{\partial}{\partial \zeta} \tag{11}$$

where  $\xi$ ,  $\zeta$  and  $\eta$  represent the coordinates of the calculation plane and correspond to the streamwise flow and the cross-sectional directions along the computational grid.

**2.4. Numerical analysis**

Calculation has been performed for all regions of the rotating U-bend, as shown in Figure 3, which shows the computational grid layout of the U-bend from above. The number of computational grid points over the entire cross-section is 21 × 21, and 446 grid points are set along the streamwise direction. Therefore, the total number of computational grids is 196,686. In the curved duct, the grids are arranged at 5° intervals.

The inlet conditions of turbulent energy and dissipation were assumed to be  $k = U_b^2 \times 10^{-5}$  and  $\varepsilon = k^{3/2}/D$ , respectively, because the inlet condition was uncertain even in the experiment. Since the present model can be classified as a high-Reynolds-number turbulent model, the wall function method is used to obtain the boundary condition for turbulent energy and dissipation at the wall. Although it has been reported that the wall function method is not suitable for separated turbulent flows, it is also true that the wall function method is an effective way to reduce the calculation time and easily set the boundary conditions. The Neumann condition is set as the outlet boundary condition. The governing equations were discretised by the differencing scheme, and QUICK (quadratic interpolation for convective kinematics) was used for the convection term. The Reynolds number is 10,000, based on the hydraulic radius and the bulk velocity.

In this numerical analysis, it is very difficult to predict well the separated turbulent flow because the

Table 2. Model constants of the pressure-strain correlation term.

$C_1^*$	$C_2^*$	$\zeta^*$	$C_1'$	$C_2'$	$\zeta'$	$C_\mu$	$\kappa$
1.4	0.44	-0.16	-0.35	0.12	-0.1	0.09	0.42

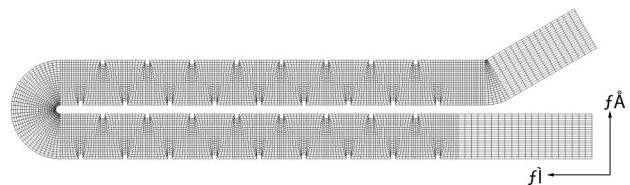


Figure 3. Computational grid.

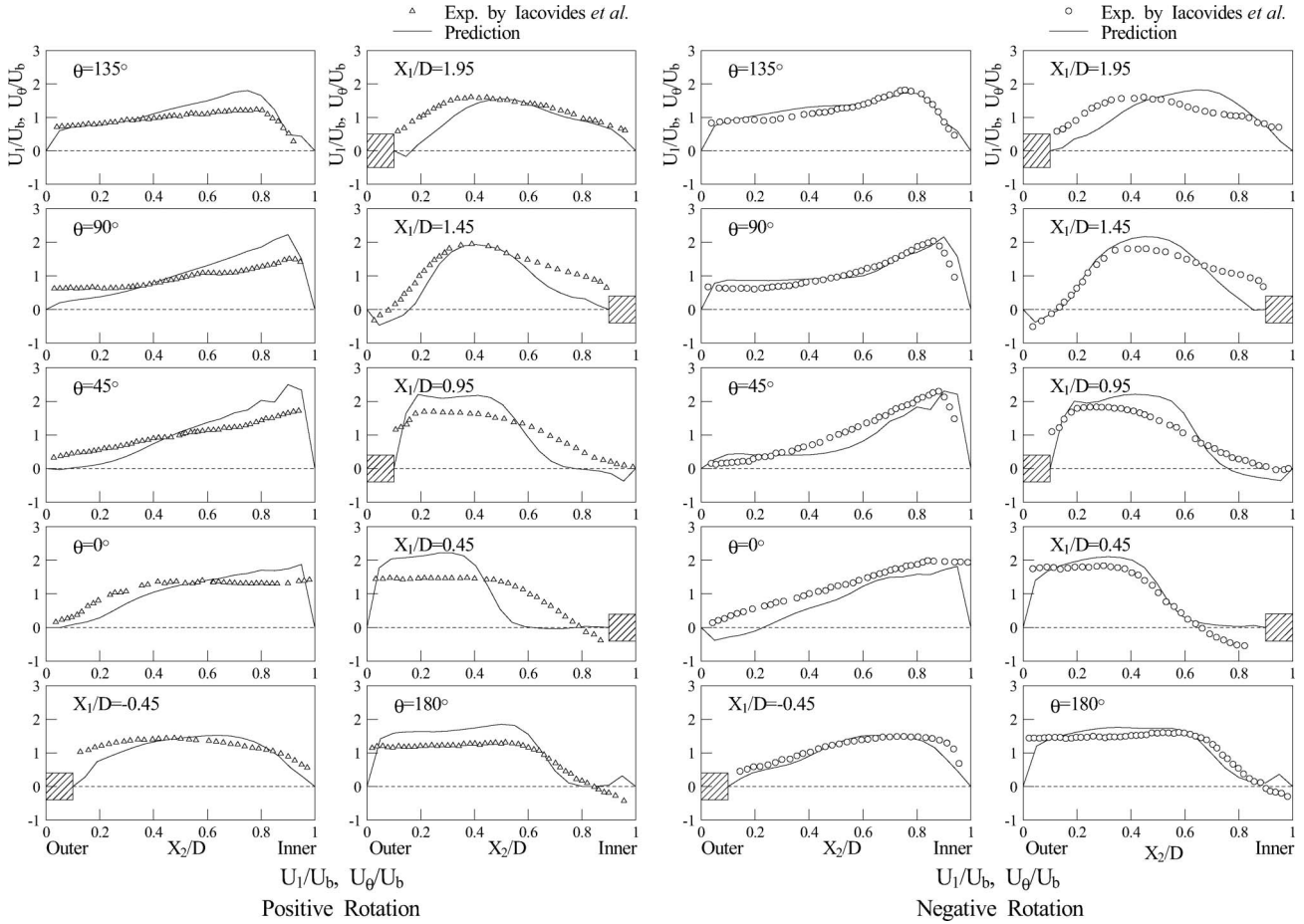


Figure 4. Streamwise velocity for positive and negative rotations.

turbulent flow is strongly influenced by not only centrifugal force but also Coriolis force induced by rotation. At the same time, it is also an important factor to predict precisely the reattachment point of the separated flow. As a preliminary calculation, Sugiyama *et al.* (2008) had predicted the separated turbulent flow in rectangular duct with a sharp 180° turn without rotation to confirm the validation of the proposed method. The calculated results of the separated turbulent flow including reattachment point show a reasonable agreement with the experiment. This calculated result suggests that the proposed method has potentiality to reproduce separated turbulent flow.

**2.5. Boundary condition for roughened wall**

It is important factor how to set boundary condition along the rib-roughened wall. There is no need to set boundary conditions of Reynolds stresses because the transport equations of Reynolds stresses

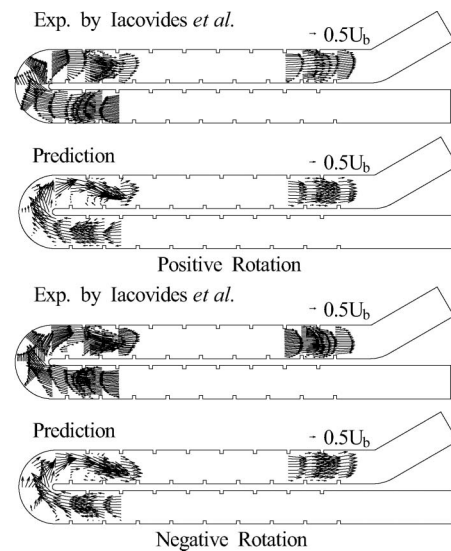


Figure 5. Velocity vectors along the flow direction.

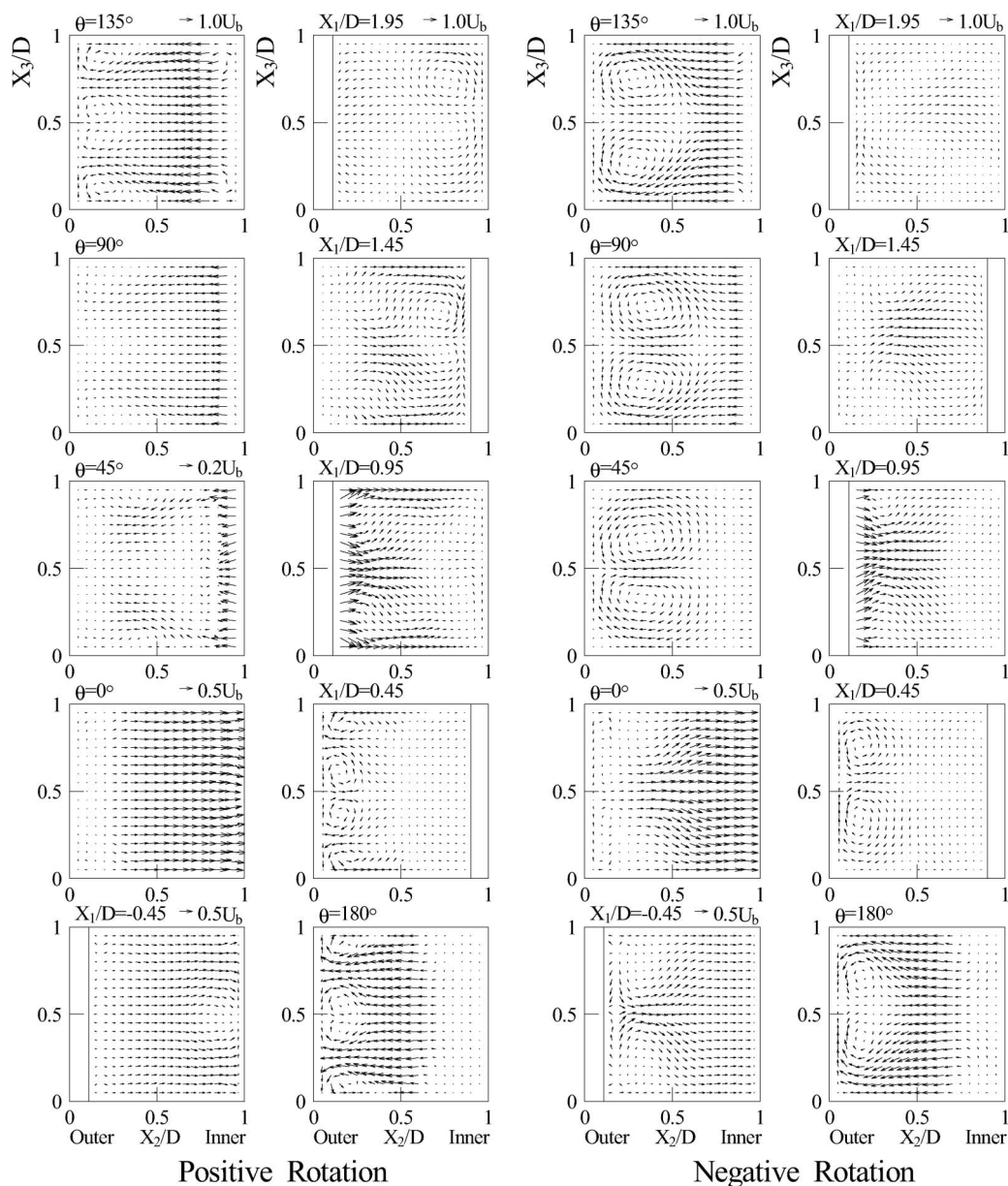


Figure 6. Calculated results of secondary flow vectors for positive and negative rotations.

are converted from differencing form into algebraic form. Therefore, special attention is paid for boundary conditions of turbulent energy and dissipation. In this numerical analysis, the wall function method was applied to not only separated turbulent flow but also region of roughened wall, which means all walls are covered with the wall function method. According to this method, friction velocity  $U_\tau$  is required in order to estimate turbulent energy and dissipation at the first grid point along the roughened wall and friction velocity is obtained from log-law velocity profile. However, the universal constant of the log-law velocity profile depends on

the situation of the roughened wall. If the universal constant has been measured in advance, the calculation is able to produce more accurate results in the turbulent flow with the roughened wall because the wall function method is derived from assuming the log-law velocity profile and local equilibrium concept which means the production of turbulent energy almost balances with that of dissipation near the wall. For example, Sugiyama *et al.* (2002) had predicted reasonably anisotropic turbulent flow in a square duct with one roughened wall by making use of the measured universal constant. In the case of this calculation, the universal constant of the log-law

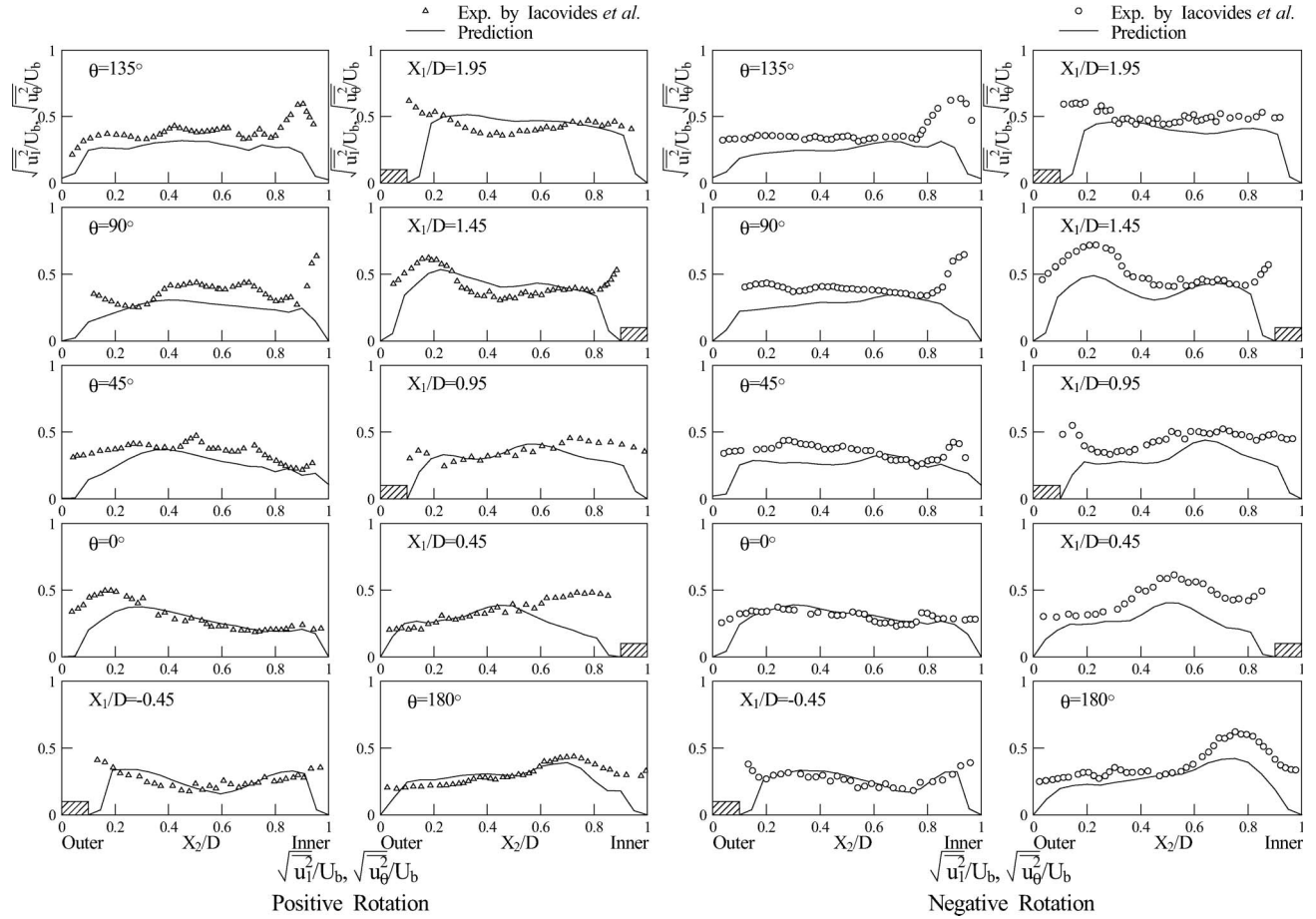


Figure 7. Streamwise normal stress  $\overline{u_1^2}$  for positive and negative rotations.

velocity profile near the roughened wall has not been measured experimentally and so the conventional form of the log-law velocity is used in calculation; i.e.

$$\frac{U_1}{U_\tau} = \frac{1}{0.42} \ln\left(\frac{U_\tau y}{\nu}\right) + 5.5. \quad (12)$$

Symbol  $y$  represents distance between the first grid point and wall.

### 3. Results and discussion

#### 3.1. Mean velocity

The calculated results for the streamwise flow velocities are compared to the experimental data at symmetric plane  $X_3/D = 0$ , as shown in Figure 4. The two left-most columns of Figure 4 show the streamwise velocity for the positive direction, and the two right-most columns of Figure 4 show the streamwise velocity for the negative rotation. The  $X_2$  axis represents the distance between the inner wall and measurement

point, and the positive direction of the  $X_2$  axis is defined as the direction from the inner wall towards the outer wall. The cross-section of  $X_1/D = -0.45$  is equivalent to the outer wall rib installed slightly upstream from the inlet of the curved duct. On the other hand, the cross-section of  $X_1/D = 0.45$  is equivalent to the inner wall rib located downstream of the outlet of the curved duct. Therefore,  $X_1/D = 0.95, 1.45$  and  $1.95$  correspond to the second, third and fourth ribs, respectively, in order as numbered from the outlet of the curved duct. In Figure 4,  $U_\theta$ ,  $U_r$  and  $U_b$  indicate the mean velocity in the  $\theta$  and  $r$  directions in the curved duct and the bulk velocity, respectively.

Based on experimental data, Iacovides *et al.* (1996) reported, as characteristic features, that the streamwise velocity has a uniform profile in the case of positive rotation, whereas in the case of negative rotation, a high streamwise velocity is generated near the inner wall. These characteristic features are caused by Coriolis effects, i.e. the Coriolis force acts from the inner wall towards the outer wall in

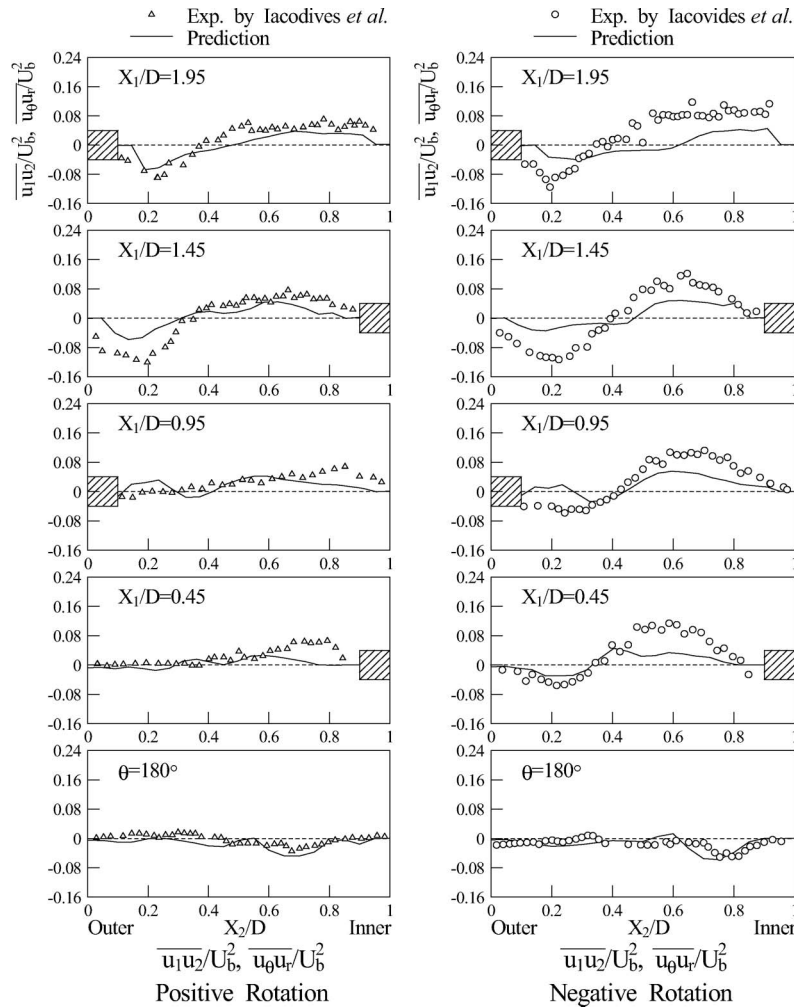


Figure 8. Shear stress  $\overline{u_{\theta}u_r}$  for positive and negative rotations.

positive rotation and from the outer wall towards the inner wall in the case of negative rotation. When the calculated velocity profile in positive rotation is compared to that in negative rotation at  $X_1/D = -0.45$ , the maximum velocity is generated closer to the inner wall in negative rotation than in positive rotation. In addition, these features are also characteristic of the velocity profile of the inlet cross-section  $\theta = 0^\circ$  of the U-bend. Here, a separated flow region is generated near the outer wall only in the case of negative rotation. The absence of the separated flow region in positive rotation is a result of the Coriolis force, which induces a high transport velocity towards the outer wall. In positive rotation, the Coriolis force acts from the inner wall towards the outer wall. The calculation shows better agreement with the experimental data in negative rotation, as compared to positive rotation. On the other hand, the calculation fails to predict the experimental

velocity profile in the separated flow region generated just downstream of the curved duct.

The calculated streamwise velocity vectors in the  $X_1 - X_2$  plane at  $X_3/D = 0$  and the experimental data, including the separated region are shown in Figure 5. In positive rotation, the calculation predicts large separated flow regions along both the inner and outer walls just downstream of the curved duct. This tendency also occurs in negative rotation. Near the inner wall, similar to the experimental result, the calculation predicts well the large separated region. Iacovides (1999) reported calculated results obtained using a differential second-moment closer model without omitting the convection term of the Reynolds stress transport equation. His results indicate a small separated flow region along the outer wall in the vicinity of the inlet cross-section of the U-duct, regardless of rotation. However, such a small separated flow is not observed in the experimental

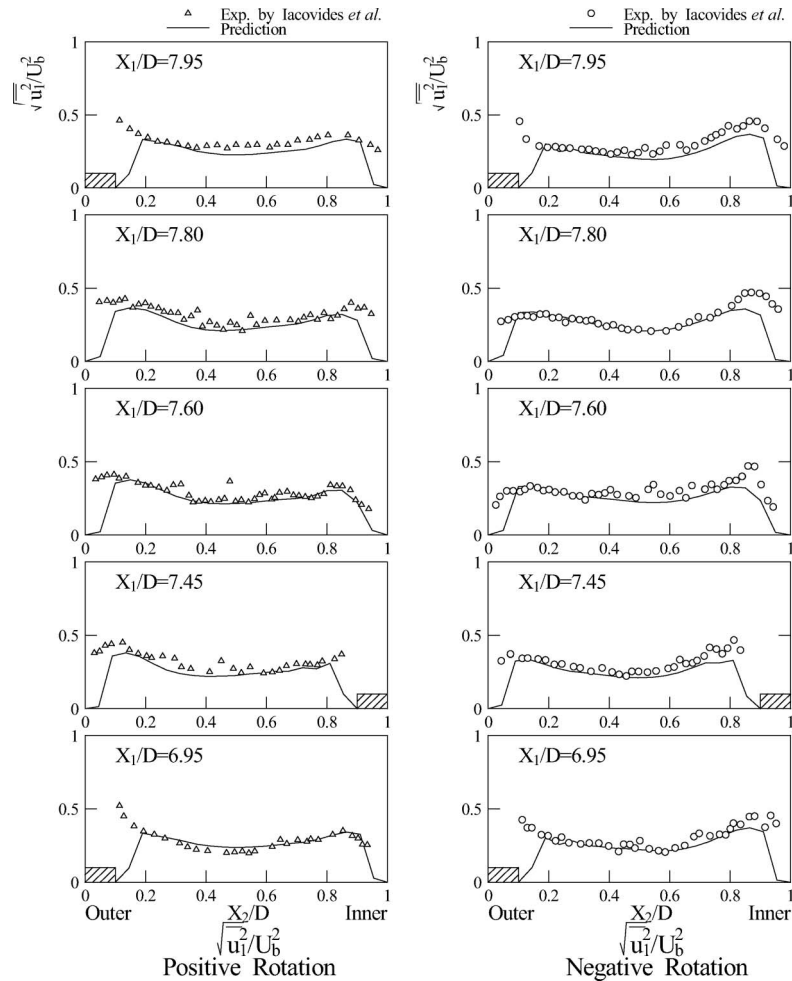


Figure 9. Streamwise normal stress  $\overline{u_1^2}$  in a straight duct.

data. In this respect, the proposed method can reproduce the experimental results more exactly in the case of positive rotation. These results suggest that the algebraic stress model may reasonably predict complicated turbulent flows. However, a detailed analysis of factors that affect calculation accuracy is necessary because there are several differences, such as the inlet length, the inlet condition, the number of grids and the differencing scheme for the convection term, between the method of Iacovides and the proposed method.

Experimental vectors along the  $\theta = 90^\circ$  line are directed upward towards the left in positive rotation and approximately upward in negative rotation. The calculated vectors in positive rotation are in agreement with the experimentally obtained vectors. On the other hand, in the case of negative rotation, the direction of the calculated vectors along the  $\theta = 90^\circ$  line changes from upward towards the right to upward towards the left, which is different from the

experimental vectors. At the same time, the experimental results suggest that the direction of the velocity vector changes from approximately upward to upward towards the left with the change from negative rotation to positive rotation. Like the experimentally obtained vectors, the calculated vectors near the outer wall along the  $\theta = 90^\circ$  line also exhibit this characteristic tendency. This characteristic tendency is attributed to the Coriolis force, which is closely related to the secondary flow.

The calculated distributions of secondary flow vectors contribute to clarify the difference of secondary flow behaviour between positive and negative rotations. Adding to this, since it is very difficult to measure exactly the secondary flow vectors at cross-sections of curved duct with rotation, the calculated results of secondary flow provide useful information to understand development of secondary flow, which lead to make the turbulent flow with heat transfer mechanism clear.

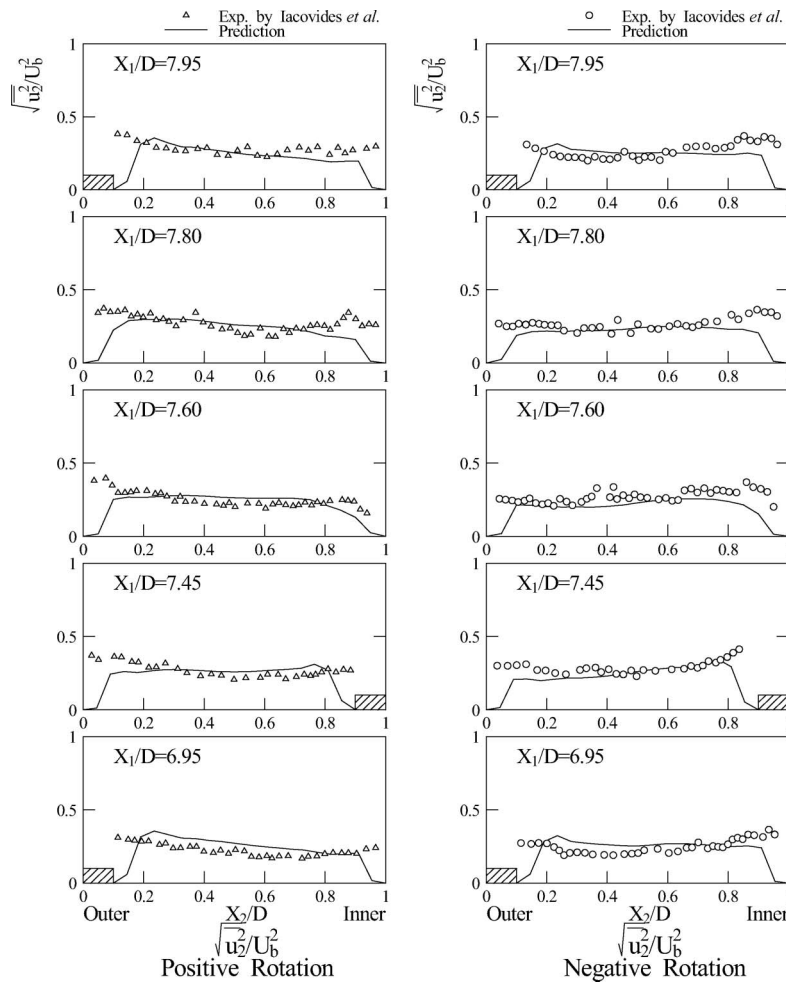


Figure 10. Horizontal normal stress  $\overline{u_2^2}$  in a straight duct.

The results for the secondary flow are arranged in two rows each for positive and negative rotations, as shown in Figure 6. Since no experimental data are available for these conditions, only calculated results are indicated at the identical location of the streamwise flow velocity as two-dimensional vectors. In the case of a curved duct, the secondary flow is generated by an imbalance between centrifugal and pressure-gradient-driven forces. However, the secondary flow in the curved duct with rotation shows a more complicated behaviour than that without rotation. When special attention is given to the curved duct region, the secondary flow is found to move uniformly from the inner wall towards the outer wall in positive rotation. In contrast, the secondary flow in the case of negative rotation is generated from the outer wall towards the inner wall along the line of  $X_3/D = 0.5$ . This tendency, which is a result of the Coriolis force, is particularly noticeable for cross-sections following the  $\theta = 45^\circ$  cross-section. Sugiyama and Watanabe (2003) predicted

the turbulent flow in the same U-bend without rotation and reported calculated results of the secondary flow vectors along the flow direction. Comparison of the secondary flow without rotation to that with rotation, as reported by Sugiyama and Watanabe (2003), confirmed that the secondary flow pattern with negative rotation is similar to that without rotation. In the case of the U-bend duct without rotation, the secondary flow is formed from the outer wall towards the inner wall because the pressure-driven force is superior to the centrifugal force. This pressure-driven force is generated by the sharp turn of the curved duct. In addition, in the case of the U-bend in negative rotation, the Coriolis force acts on the fluid flow from the outer wall towards the inner wall. Therefore, a similar secondary flow pattern suggests that the acting direction of the Coriolis force agrees with that of the pressure-driven force. This indicates that the intensity of the secondary flow in negative rotation is much greater than that without rotation, because the Coriolis force is added to the

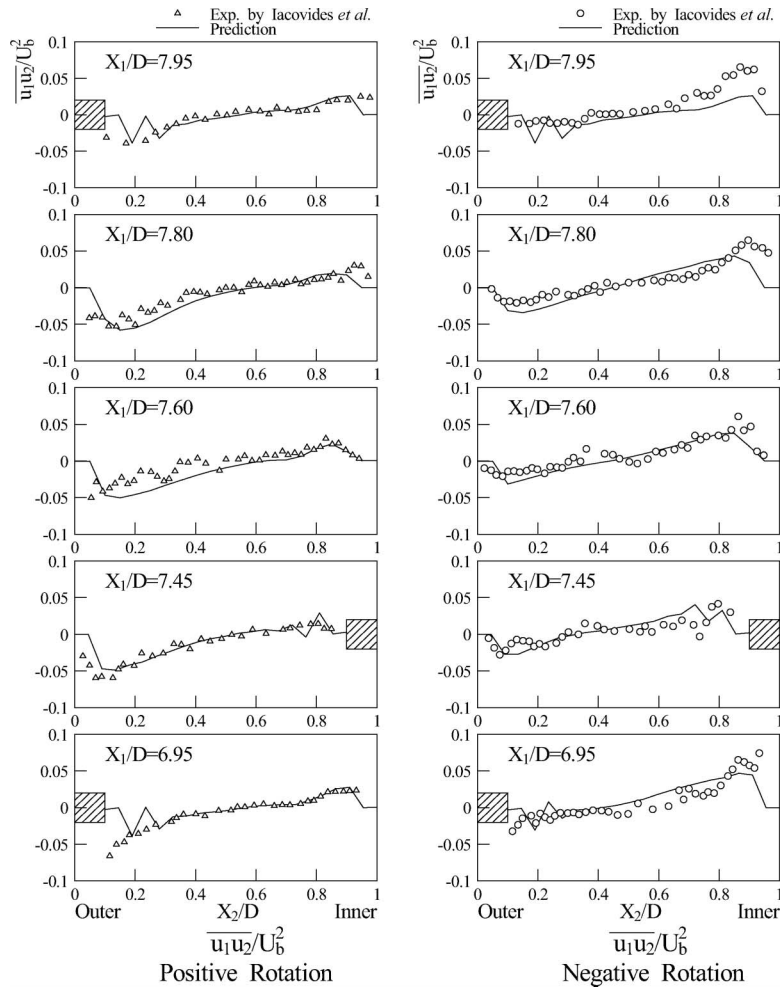


Figure 11. Shear stress  $\overline{u_1 u_2}$  in a straight duct.

pressure-driven force. These calculated results for the secondary flow imply that the direction of rotation has a significant impact on the heat transfer in the rotating duct with roughened walls.

### 3.2. Reynolds stress distributions

The streamwise fluctuating velocity for positive (two left-most columns) and negative (two right-most columns) rotations is shown in Figure 7. In Figure 7, stresses  $u_1^2$  and  $u_\theta^2$  represent the streamwise fluctuating velocity in straight and curved ducts, respectively. The calculated and experimental results are normalised by the bulk velocity. The experimental and calculated results at  $X_1/D = -0.45$  indicate that the distributions of the streamwise fluctuating in positive rotation are different from those in negative rotation. The production term of the streamwise fluctuating velocity induced by rotation, which is the fourth term of right-hand side of the Reynolds transport equation, i.e.

Equation (2), is the product of the angular velocity of the duct and the shear stress  $-\overline{u_1 u_2}$ . This means that the stress  $-\overline{u_1 u_2}$  affects the production of the streamwise fluctuation.

Moreover, the experimental result for the  $\theta = 0^\circ$  cross-section in positive rotation indicates that the maximum value of the streamwise fluctuating velocity is generated near the outer wall. This characteristic feature can be reproduced by the proposed calculation. In contrast, the experimental data show a peak value in the vicinity of the inner wall side at the  $\theta = 90^\circ$  and  $135^\circ$  cross-sections, whereas this peak value is not predicted by the calculation. These differences between calculated and experimental results imply that it is necessary to correctly predict the separation and reattachment points of the separated flow.

The results for the shear stress  $-\overline{u_1 u_2}$  in positive and negative rotation are shown in Figure 8. The experimental data in negative rotation indicate that the absolute value of the shear stress increases gradually as

the flow develops. On the other hand, a remarkable increase in absolute shear stress is not observed in positive rotation. When the results are compared in detail, the proposed method tends to underestimate the experiment in negative rotation. This tendency probably results from the failure to precisely predict the streamwise velocity in the separated flow region. In the turbulent flow with separation, it is important to predict exactly the separation and reattachment points of the separated flow because the calculation cannot correctly reproduce the streamwise velocity profile after the separated flow unless the predicted reattachment point is in good agreement with the experimentally observed value. This discrepancy with respect to the reattachment point affects the prediction accuracy for the shear stress.

The streamwise and horizontal fluctuating velocities and the shear stress  $-\overline{u_1 u_2}$  in a straight duct located downstream of a curved duct are shown in Figures 9–11, respectively. All of the cross-sections in the figures are situated after  $X_1/D = 6.95$ , which corresponds to the 14th rib, as counted from the outlet of the curved duct. Since the effect of the separated region on flow behaviour decays gradually as the flow moves downstream of the curved duct, the calculated results are in good agreement with the experimental results, as shown in Figures 9–11. At the same time, these results indicate that the influence of the separated region disappears after the  $X_1/D = 6.95$  cross-section.

#### 4. Conclusions

A numerical analysis has been performed for a three-dimensional developing turbulent flow in a rotating U-bend with rib-roughened walls. In this calculation, an algebraic Reynolds stress model is used to precisely predict Reynolds stresses, and a boundary-fitted coordinate system is introduced as a coordinate transformation method. Calculated results were compared quantitatively to the experimental data reported by Iacovides *et al.* (1996) in order to confirm the validity of the proposed method and to clarify the flow mechanism theoretically. The numerical analysis revealed the following:

- (1) The proposed method can qualitatively predict the experimental features of streamwise velocity in a rotating U-duct with roughened walls. For example, the proposed method can reproduce the uniform streamwise velocity in positive rotation and the high-velocity profile near the inner wall in negative rotation due to the Coriolis force.
- (2) The experimental results show that separated flow is generated near the outer wall just after

the outlet of the curved duct, regardless of the direction of rotation. The present method also predicts this separated flow, although the calculation tends to predict the separated flow region as being larger than the experimentally determined separated flow region.

- (3) As for the secondary flow, the calculated results suggest that the secondary flow pattern depends greatly on the direction of rotation and exhibits complicated flow behaviour as the flow develops. The secondary flow pattern in negative rotation is similar to that without rotation, and the secondary flow direction in negative rotation is opposite that in positive rotation.
- (4) The experimental distribution of the streamwise fluctuating velocity exhibits a maximum peak value near the inner wall, regardless of the direction of rotation. The calculation cannot predict this characteristic feature well.
- (5) The calculation fails to predict exactly the distributions of normal and shear stresses in the flow region just after the outlet cross-section of the curved duct because the predicted reattachment point of the separated flow differs from the experimentally observed value. However, the calculation predicts well the normal and shear stresses downstream in the straight duct because the influence of the separated flow disappears downstream in the straight duct.
- (6) Although the numerical and experimental results are not in perfect agreement, the proposed algebraic Reynolds stress model is applicable to the complicated turbulent flow in the rotating U-bend with roughened walls.

#### References

- Buggraf, F., 1970. Experimental heat transfer and pressure drop with two-dimensional discrete turbulent promoters applied to two opposite walls of square duct. In: A.E. Bergles and R.L. Webb, eds. *Augmentation of convective heat and mass transfer*. New York: ASME, 70–79.
- Champagne, F.H., Harris, V.G., and Corrisn, S., 1970. Experimental on nearly homogeneous turbulent shear flow. *Journal of Fluid Mechanics*, 41, 81–139.
- Ekkad, S.V., Pamula, G., and Acharaya, S., 2000. Influence of crossflow-induced swirl and impingement on heat transfer in an internal coolant passage of a turbine airfoil. *Journal of Heat Transfer*, 122, 587–597.
- Gessner, F.B. and Eppich, H.M., 1981. A near-wall pressure-strain model for turbulent corner flows. *Proceedings of Third Symposium on Turbulent Shear Flows*, 9–11 September, University of California, Davis, CA, 25–32.

- Guleren, K.M. and Turan, A., 2007. Validation of large-eddy simulation of strongly curved stationary and rotating U-duct flows. *International Journal of Heat and Fluid Flow*, 28, 909–921.
- Han, J.C., Chanda, P.R., and Lau, S.C., 1988. Local heat/mass transfer distributions around sharp 180 degree turns in two-pass smooth and rib-roughened channels. *Journal of Heat Transfer*, 110, 91–98.
- Hsieh, S.-S., Chen, P.-J., and Chin, H.-J., 1999. Turbulent flow in a rotating two pass smooth channel. *Journal of Fluid Engineering*, 121, 725–734.
- Iacovides, H., 1999. The computation of turbulent flow through stationary and rotating U-bends with rib-roughened surface. *International Journal for Numerical Methods in Fluids*, 29, 865–876.
- Iacovides, H., et al., 1996. LDA study of the flow developing through an orthogonally rotating U-bend of strong curvature and rib roughened walls. In: W. Rodi and G. Bergeles, eds. *Engineering Turbulence Modelling and Experiments*. Vol. 3. Oxford: Elsevier Science Ltd, 561–570.
- Iacovides, H., et al., 1999. An experimental study of a rib-roughened rotating U-bend flow. *Experimental Thermal and Fluid Science*, 19, 151–159.
- Iacovides, H. and Raisee, M., 1999. Recent progress in the computation of flow and heat transfer in internal cooling passage of turbine blades. *International Journal of Heat and Fluid Flow*, 20, 320–328.
- Jang, Y.-U., Chen, H.-C., and Han, J.-C., 2001. Computation of flow and heat transfer in two-pass channels with 60 degree ribs. *Journal of Heat Transfer*, 121, 563–575.
- Lauder, B.E., Reece, G.J., and Rodi, W., 1975. Progress in the development of a Reynolds stress turbulent closure. *Journal of Fluid Mechanics*, 22, 537–566.
- Lin, Y.-L., et al., 2001. A numerical study of flow and heat transfer in a smooth and ribbed U-duct with and without rotation. *Journal of Heat Transfer*, 123, 219–232.
- Rodi, W., 1976. A new algebraic relation for calculating the Reynolds stresses. *Zeitschrift fuer angewandte Mathematik und Mechanik*, 56, 219–221.
- Sugiyama, H., et al., 2002. Calculation of turbulent heat flux distributions in a square duct with one roughened wall by means of algebraic heat flux models. *International Journal of Heat and Fluid Flow*, 23, 13–21.
- Sugiyama, H. and Watanabe, C., 2003. Numerical analysis of developing turbulent flow in a U-bend of strong curvature with rib-roughened walls. *Transactions of Atomic Energy Society of Japan*, 2–1, 24–31 (in Japanese).
- Sugiyama, H. and Hitomi, D., 2005. Numerical analysis of developing turbulent flow in a 180° bend tube by an algebraic Reynolds stress model. *International Journal for Numerical Methods in Fluids*, 47, 1431–1449.
- Sugiyama, H., Tanaka, T., and Mukai, H., 2008. Numerical analysis of turbulent flow separation in a rectangular duct with a sharp 180-degree turn by algebraic Reynolds stress model. *International Journal for Numerical Methods in Fluids*, 56, 2207–2228.